
GROUPKAN: RETHINKING NONLINEARITY WITH GROUPED SPLINE-BASED KAN MODELING FOR EFFICIENT MEDICAL IMAGE SEGMENTATION

Guojie Li

School of Robotics, Xi'an Jiaotong-Liverpool University

Suzhou, Jiangsu 215000, China

Department of Computer Science, University of Liverpool, Liverpool L69 3BX, UK

Anwar P.P. Abdul Majeed

School of Robotics, Xi'an Jiaotong-Liverpool University, Suzhou, Jiangsu 215000, China
Faculty of Engineering and Technology, Sunway University, Selangor Darul Ehsan 47500, Malaysia

Muhammad Ateeq

School of Internet of Things, Xi'an Jiaotong-Liverpool University
Suzhou, Jiangsu 215000, China

Anh Nguyen

Department of Computer Science, University of Liverpool
Liverpool L69 3BX, United Kingdom

Fan Zhang*

School of Robotics, Xi'an Jiaotong-Liverpool University
Suzhou, Jiangsu 215000, China

ABSTRACT

Medical image segmentation requires models that are accurate, lightweight, and interpretable. Convolutional architectures lack adaptive nonlinearity and transparent decision-making, whereas Transformer architectures are hindered by quadratic complexity and opaque attention mechanisms. U-KAN addresses these challenges using Kolmogorov-Arnold Networks, achieving higher accuracy than both convolutional and attention-based methods, fewer parameters than Transformer variants, and improved interpretability compared to conventional approaches. However, its $\mathcal{O}(C^2)$ complexity due to full-channel transformations limits its scalability as the number of channels increases. To overcome this, we introduce GroupKAN, a lightweight segmentation network that incorporates two novel, structured functional modules: (1) *Grouped KAN Transform*, which partitions channels into G groups for multivariate spline mappings, reducing complexity to $\mathcal{O}(C^2/G)$, and (2) *Grouped KAN Activation*, which applies shared spline-based mappings within each channel group for efficient, token-wise nonlinearity. Evaluated on three medical benchmarks (BUSI, GlaS, and CVC), GroupKAN achieves an average IoU of 79.80%, surpassing U-KAN by +1.11% while requiring only 47.6% of the parameters (3.02M vs 6.35M), and shows improved interpretability. **Code available at:** <https://github.com/liguojie09/GroupKAN>

Keywords Computer Vision · Medical Image Segmentation · Kolmogorov-Arnold Networks ·

*Corresponding author: Fan.Zhang@xjtlu.edu.cn

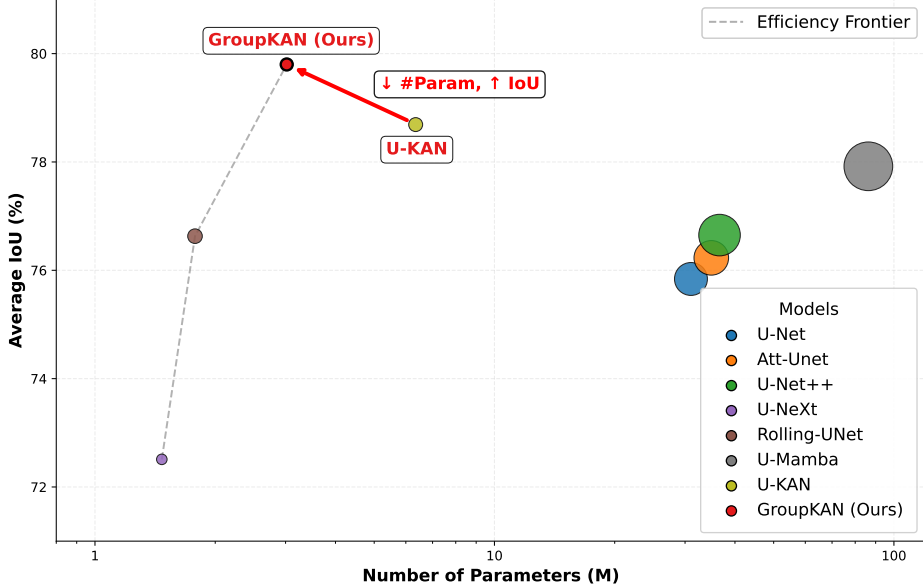


Figure 1: Accuracy–complexity trade-off in medical segmentation: IoU (%) vs. number of parameters (M) among common backbone models. Marker size reflects each model’s computational cost, with areas proportional to their GFLOPs. The dashed line indicates the efficiency frontier. Our GroupKAN (red circle) improves IoU by 1.11% over U-KAN, with 47.6% of U-KAN’s parameters.

1 Introduction

Medical image segmentation is critical for clinical diagnosis and treatment planning [1, 2], yet existing deep learning models struggle to balance accuracy, compactness, and interpretability under real-world clinical constraints [3, 4, 5]. Although existing methods yield accurate segmentation results, their high computational cost and opaque decision processes hinder deployment in real-world, resource-limited medical environments.

Convolutional neural networks, such as U-Net [6], have long served as the backbone of medical image segmentation systems due to their strong inductive biases, which help generalization in data-limited regimes. However, their limited expressiveness and lack of adaptive nonlinearity hinder their ability to model complex structures, motivating the need for more flexible and interpretable alternatives [7, 8]. In contrast, Transformer-based methods abandon local inductive biases in favor of global self-attention, enabling long-range context modeling but suffering from quadratic complexity and data inefficiency [9, 10, 11]. More recent models such as Mamba [12] leverage state-space formulations to model long-range dependencies with linear-time complexity. However, their architectural complexity and limited application to dense prediction tasks restrict their effectiveness in segmentation scenarios.

To enhance interpretability, U-KAN [13] integrates Kolmogorov-Arnold Networks (KANs) [14] via full-channel spline transformations applied across feature dimensions. While improving segmentation accuracy and interpretability, this design incurs a parameter complexity of $\mathcal{O}(C^2)$, resulting in quadratic growth in model size as the channel dimension increases, which poses challenges for scalability and deployment in resource-limited settings.

To address these limitations, we propose **GroupKAN**, a lightweight architecture consisting of two key innovations: (1) *Grouped KAN Transform* (GKT), which partitions channels into G independent groups and applies group-specific spline operators within each group to model channel-wise interactions. This structured design reduces the transformation’s parameter complexity from $\mathcal{O}(C^2)$ to $\mathcal{O}(C^2/G)$, significantly lowering model size while preserving representational capacity; (2) *Grouped KAN Activation* (GKA), a novel spline-based pointwise nonlinearity where all channels in the same group share the same spline function. This promotes interpretability by enabling structured per-token activations while maintaining functional diversity across groups.

GroupKAN revisits functional modeling by integrating group-aware spline operations into a lightweight architecture, achieving simultaneous improvements in interpretability, lightweight design, and accuracy for medical image segmentation. (see Fig. 1). Specifically, our contributions are:

- We propose **GroupKAN**, a lightweight backbone for medical image segmentation that integrates group-aware spline modeling. GroupKAN employs Kolmogorov–Arnold Networks to jointly model token-level activations and channel-wise transformations, unifying these processes in an interpretable and compact framework.
- We propose **Grouped KAN Transform (GKT)**, a computationally efficient operator that performs multivariate spline mappings within channel groups. This reduces parameter complexity from $\mathcal{O}(C^2)$ to $\mathcal{O}(C^2/G)$, while maintaining the ability to model rich inter-channel dependencies.
- We propose **Grouped KAN Activation (GKA)**, a spline-based nonlinearity that applies shared univariate functions within channel groups after patch embedding. This design enables parameter-efficient token-wise activations.
- We validate GroupKAN on three medical segmentation benchmarks (BUSI, GlaS, and CVC), where it achieves an average IoU improvement of 1.11% over U-KAN with only 3.02M parameters, delivering both quantitative and qualitative gains as well as more interpretable predictions.

2 Related Work

2.1 Architectures for Medical Segmentation

U-shaped architectures, exemplified by U-Net [6], are widely used as backbones for medical image segmentation due to their symmetric encoder-decoder structure and skip connections that support multi-scale feature fusion. Numerous extensions have since improved upon this design by enhancing skip pathways [15, 16], incorporating attention mechanisms [17, 18, 19], and updating convolutional components [20].

More recently, lightweight architectures such as Rolling U-Net [21] combine convolutional encoders with MLP-inspired modules to improve long-range dependency modeling while maintaining efficiency. In parallel, models like U-Mamba [22] incorporate Mamba-style sequence modeling to enhance global representation learning. However, most existing efforts concentrate on architectural modifications, leaving nonlinear transformation design relatively underexplored.

2.2 Kolmogorov Arnold Networks and Functional Modeling

KANs [14] approximate functions via learnable spline compositions, offering strong interpretability and expressivity with fewer parameters. U-KAN [13] introduces functional activations into U-shaped networks by inserting spline-based KAN modules, achieving strong results in both segmentation and generation. However, its global channel-wise mappings incur high parameter and compute cost, especially as channel dimensions grow. This highlights the need for more efficient functional modeling.

Recent works have explored convolutional KANs [23, 24], replacing linear convolution kernels with spline-based nonlinear filters to improve representational capacity and accuracy. However, these approaches often introduce substantial parameter and compute overhead and lack structured group-wise design. Consequently, the potential of group-aware spline transformations for parameter-efficient segmentation remains underexplored.

2.3 Nonlinear Activations

Standard activation functions such as ReLU [25] and GELU [26] are computationally efficient but fixed, which may limit the nonlinear modeling capacity of deep networks. To improve flexibility, recent works have introduced learnable alternatives. Truncated Ensemble Linear Unit (TeLU) [27] formulates activations as trainable combinations of truncated ReLUs, enabling bounded and smooth transitions. Gompertz Linear Unit (GoLU) [28] introduces an asymmetric activation based on the Gompertz function, defined as $f(x) = x \text{Gompertz}(x)$, which enhances gradient flow for positive inputs while smoothly suppressing negatives. GoLU leverages this inherent asymmetry to improve learning dynamics and convergence stability in deep networks. In parallel, architectural studies suggest that inserting nonlinear activations immediately after patch embedding enhances early-stage representational capacity. Notably, CvT [29] and PVTv2 [30] empirically demonstrate that post-projection activations (e.g., GELU) benefit dense prediction tasks. However, these activations are applied independently per neuron and lack awareness of spatial or channel-level structure.

3 Method

Fig. 2 presents the overall architecture of **GroupKAN**, a lightweight network tailored for medical image segmentation. The design adopts a symmetric encoder-decoder structure, where the encoder comprises three convolutional stages

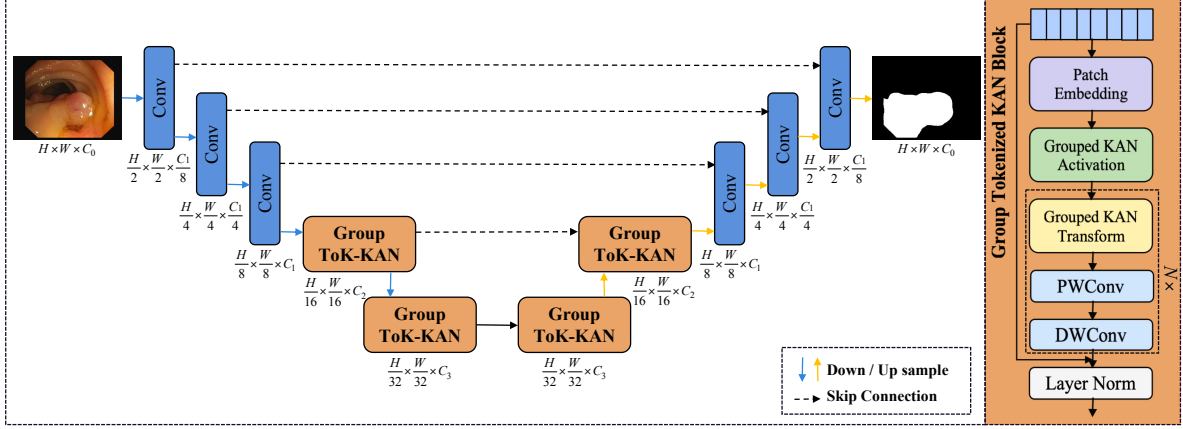


Figure 2: Overview of the GroupKAN pipeline. The encoder extracts features through convolutional blocks. In the bottleneck, each Group ToK-KAN block applies patch embedding and Grouped KAN Activation, followed by N repeated Grouped KAN Transforms with pointwise and depthwise convolutions. The decoder mirrors the encoder with upsampling and skip connections to produce the final segmentation map.

with output channel dimensions of $C_1/8$, $C_1/4$, and C_1 . Each stage progressively halves the spatial resolution while capturing increasingly abstract features.

Following the convolutional encoder, feature maps are processed by a series of **Grouped Tokenized KAN** (Group ToK-KAN) blocks. Each block begins with a patch embedding that reshapes the spatial feature maps into $B \times N \times C$ tokens, where C denotes the channel dimension. A **Grouped KAN Activation** is then applied by splitting the C channels into G groups and applying shared spline-based univariate activations within each group, enabling learnable and efficient token-level nonlinearities. This is followed by a **Grouped KAN Transform**, iterated for N steps, where each iteration uses group-wise fully connected KAN layers to transform intra-group channel features, alongside pointwise and depthwise convolutions to support cross-group communication and spatial interaction. Two ToK-KAN blocks are used in the bottleneck stage, operating at intermediate channel dimensions C_2 and C_3 .

The decoder mirrors the encoder structure, progressively upsampling and refining features through convolutional blocks. Skip connections from the encoder facilitate multi-scale information fusion. Decoding stages operate on channel dimensions C_3 , C_2 , C_1 , $C_1/4$, and $C_1/8$, and the final output is projected to the segmentation map via a 1×1 convolution.

3.1 KAN as Interpretable Functional Modules

Kolmogorov–Arnold Networks (KANs) [14] reformulate neural computation by replacing fixed-weight projections and static activations with learnable univariate spline functions. This design is inspired by the Kolmogorov–Arnold representation theorem [31], which states that any multivariate function can be decomposed into a finite sum of univariate functions and addition. By decoupling transformation and nonlinearity, KANs provide a unified functional modeling paradigm with enhanced expressivity and interpretability.

Each KAN layer applies a matrix of trainable spline-based operators Φ_k to the input:

$$\mathbf{Z}_{k+1} = \Phi_k \mathbf{Z}_k, \quad (1)$$

where each $\phi_{q,p} : \mathbb{R} \rightarrow \mathbb{R}$ is a learnable univariate spline. This formulation enables compact and interpretable representations with strong functional fidelity, offering a compelling alternative to traditional MLPs, particularly for dense prediction tasks such as medical image segmentation.

In our framework, KAN fulfills two complementary roles: (1) **Grouped KAN Transform (GKT)**, where structured spline mappings are applied within channel groups to model inter-channel dependencies; and (2) **Grouped KAN Activation (GKA)**, where grouped univariate spline functions modulate patch embeddings to enhance token-wise representation. These roles reflect our architectural strategy and enable GroupKAN to effectively replace MLP and attention modules within segmentation networks, yielding both interpretability and a lightweight design.

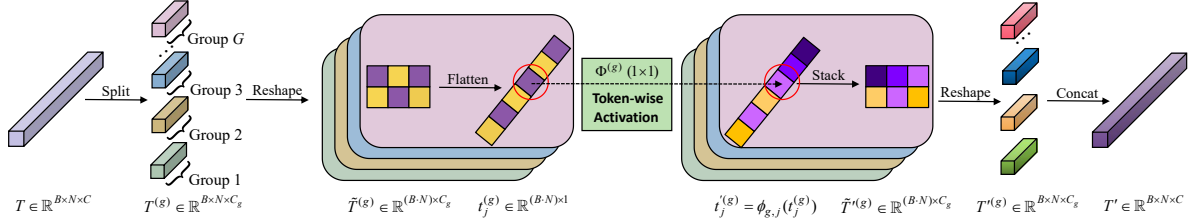


Figure 3: Illustration of Grouped KAN Activation. Given token embeddings $T \in \mathbb{R}^{B \times N \times C}$, we split the channel dimension into G groups, each reshaped to $(B \cdot N) \times C_g$. A 1D KAN function $\Phi^{(g)}$ is then applied independently to each scalar dimension in every group. The outputs are reshaped and concatenated to yield the activated representation $T' \in \mathbb{R}^{B \times N \times C}$.

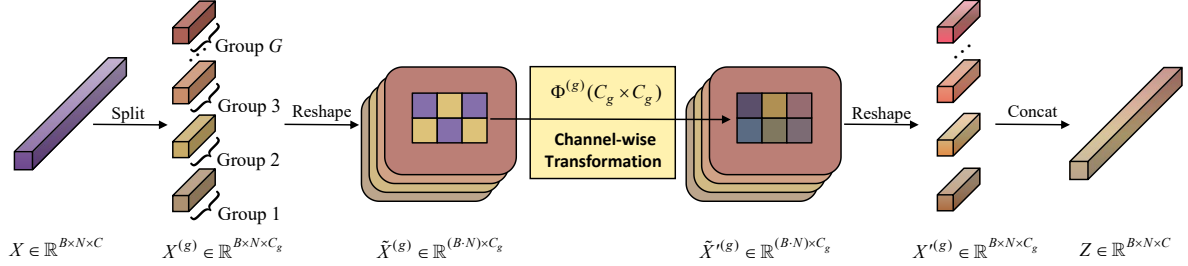


Figure 4: Illustration of Grouped KAN Transform. The input feature $X \in \mathbb{R}^{B \times N \times C}$ is divided into G groups along the channel dimension. Each group is reshaped to $(B \cdot N) \times C_g$ and passed through a nonlinear transformation $\Phi^{(g)}$ with learnable mappings of size $C_g \times C_g$. The transformed outputs are reshaped and concatenated to form the output $Z \in \mathbb{R}^{B \times N \times C}$.

3.2 Group Tokenized KAN

To initiate the Group Tokenized KAN phase, we first convert 2D feature maps into a sequence of patch tokens. A 3×3 convolution with stride 2 is applied to the input $X \in \mathbb{R}^{B \times C_0 \times H \times W}$, yielding intermediate features $F \in \mathbb{R}^{B \times C \times H' \times W'}$. These are reshaped into a token sequence $T \in \mathbb{R}^{B \times N \times C}$, where $N = H' \cdot W'$. We retain the convolution-based embedding strategy from U-KAN [13], which encodes local and positional priors via receptive fields, and demonstrates greater robustness to input resolution variations compared to flatten-then-project alternatives.

3.2.1 Grouped KAN Activation (GKA).

To enhance token-level expressiveness, we introduce a **GKA** module after patch embedding (see Fig. 3). Given the input sequence $T \in \mathbb{R}^{B \times N \times C}$, we divide the channel dimension into G groups of size $C_g = C/G$, yielding group-wise features $T^{(g)} \in \mathbb{R}^{B \times N \times C_g}$.

Each group is reshaped to a 2D matrix $\tilde{T}^{(g)} \in \mathbb{R}^{(B \cdot N) \times C_g}$. Then, as shown in the Flatten step, we extract each scalar feature as a column vector $t_j^{(g)} \in \mathbb{R}^{(B \cdot N) \times 1}$, and apply a token-wise 1D spline function $\phi_{g,j}(\cdot)$ to obtain $t_j'^{(g)} = \phi_{g,j}(t_j^{(g)})$.

This operation corresponds to a diagonal variant of Eq. 1, where each $\Phi^{(g)}$ comprises C_g independent (1×1) operators. The Stack operation then reconstructs the group as $\tilde{T}'^{(g)} \in \mathbb{R}^{(B \cdot N) \times C_g}$, which is reshaped to $T'^{(g)} \in \mathbb{R}^{B \times N \times C_g}$. All group outputs are finally concatenated to yield the activated sequence $T' \in \mathbb{R}^{B \times N \times C}$.

In contrast to conventional activations (e.g., ReLU or GELU) applied after early convolutions, our token-wise spline nonlinearity allows structured, group-aware transformation at the embedding level, improving token-level flexibility and expressiveness.

Methods	BUSI [32]		GlaS [33]		CVC [34]	
	IoU↑	F1↑	IoU↑	F1↑	IoU↑	F1↑
U-Net (Ronneberger et al. 2015)	57.36±4.61	72.41±3.37	86.51±1.13	92.68±0.82	83.66±1.03	91.02±0.87
Att-Unet [17]	57.62±3.93	72.77±3.14	86.67±1.25	92.77±0.77	84.39±0.68	91.52±0.34
U-Net++ [15]	58.25±3.58	73.23±2.76	87.13±0.82	93.02±0.47	84.57±1.33	91.66±0.97
U-NeXt [20]	58.27±1.56	73.38±1.77	83.64±1.02	90.98±0.52	75.62±1.08	86.21±0.87
Rolling-UNet [21]	60.23±1.23	75.05±1.65	86.53±0.87	92.50±0.74	83.12±1.38	90.79±1.12
U-Mamba [22]	61.79±3.54	76.13±3.27	87.08±0.52	93.11±0.37	84.88±0.63	91.74±0.44
U-KAN [13]	63.41±2.67	76.51±2.88	87.51±0.39	93.29±0.18	85.14±0.67	91.99±0.36
GroupKAN (Ours)	65.18±2.73	78.22±2.72	87.91±0.36	93.66±0.19	86.31±0.73	92.35±0.64

Table 1: Quantitative segmentation results on BUSI, GlaS, and CVC-ClinicDB. GroupKAN consistently achieves the best IoU and F1 scores, outperforming convolution-based, attention-based, and function-based baselines.

3.2.2 Grouped KAN Transform (GKT).

GKT extends the design of Grouped KAN Activation (GKA) from 1×1 token-wise activation to structured $C_g \rightarrow C_g$ channel transformations. While both modules adopt a group-wise spline framework (see Fig. 3 and Fig. 4), GKT enables richer intra-group modeling by applying full spline matrices within each group.

Given input $X \in \mathbb{R}^{B \times N \times C}$, we divide the channel dimension into G groups of size $C_g = C/G$, yielding $X^{(g)} \in \mathbb{R}^{B \times N \times C_g}$. Each group is reshaped into $\tilde{X}^{(g)} \in \mathbb{R}^{(B \cdot N) \times C_g}$ and passed through a learnable nonlinear mapping:

$$\tilde{X}'^{(g)} = \Phi^{(g)}(\tilde{X}^{(g)}), \quad \Phi^{(g)} = [\phi_1^{(g)}, \dots, \phi_{C_g}^{(g)}], \quad (2)$$

where each $\phi_j^{(g)} : \mathbb{R} \rightarrow \mathbb{R}$ is a spline-based function, forming a $C_g \rightarrow C_g$ transformation per group. The outputs are reshaped to $X'^{(g)} \in \mathbb{R}^{B \times N \times C_g}$ and concatenated as $Z = \text{Concat}_{g=1}^G X'^{(g)} \in \mathbb{R}^{B \times N \times C}$.

To facilitate cross-group communication and spatial interaction, we apply a pointwise convolution followed by nonlinearity and depthwise convolution:

$$Y = \text{DWConv}(\sigma(\text{PWConv}(Z))). \quad (3)$$

This process is repeated N times within each Group ToK-KAN block to progressively enrich channel-wise features. Compared to a standard full-channel KAN with $\mathcal{O}(C^2)$ complexity, the grouped variant reduces the cost to $\mathcal{O}(C^2/G)$ while maintaining expressive power within groups.

To stabilize optimization and retain identity mapping, we apply a residual connection and LayerNorm:

$$\hat{Y} = Y + X, \quad \text{Output} = \text{LayerNorm}(\hat{Y}). \quad (4)$$

The resulting output is forwarded to the next transformation stage.

4 Experiments

4.1 Datasets

To ensure fair comparison with prior work, we evaluate GroupKAN on the same datasets used in U-KAN [13], including BUSI, GlaS, and CVC-ClinicDB. These benchmarks span diverse medical imaging modalities, covering ultrasound, histopathology, and colonoscopy segmentation tasks.

BUSI [32] contains 780 breast ultrasound images annotated for tumor segmentation across benign, malignant, and normal cases. The dataset exhibits strong speckle noise and low contrast. All images are resized to 256×256 .

GlaS [33] consists of 245 histology images for colorectal gland segmentation. It features high glandular variability and structural deformation, particularly between benign and malignant samples. Images are resized to 512×512 .

CVC-ClinicDB [34] contains 612 colonoscopy frames with pixel-level polyp annotations. It involves significant illumination changes and scale variation. Images are resized to 256×256 .

Methods	Average Seg.		Efficiency	
	IoU \uparrow	F1 \uparrow	Gflops	Params (M)
U-Net [6]	75.84 \pm 2.26	85.37 \pm 1.69	436.94	31.04
Att-Unet [17]	76.23 \pm 1.95	85.69 \pm 1.42	531.78	34.9
U-Net++ [15]	76.65 \pm 1.91	85.97 \pm 1.40	1109	36.6
U-NeXt [20]	72.51 \pm 1.22	83.52 \pm 1.05	4.58	1.47
Rolling-UNet [21]	76.63 \pm 1.16	86.11 \pm 1.17	16.82	1.78
U-Mamba [22]	77.92 \pm 1.56	87.00 \pm 1.36	2087	86.3
U-KAN [13]	78.69 \pm 1.24	87.26 \pm 1.14	14.02	6.35
GroupKAN (Ours)	79.80\pm1.27	88.07\pm1.19	7.72	3.02

Table 2: Average segmentation performance and model complexity on BUSI, GlaS, and CVC-ClinicDB. GroupKAN achieves higher IoU and F1 than established backbone models while maintaining a notably lower parameter count and FLOPs to U-KAN.

4.2 Implementation Details

All experiments were conducted using PyTorch on a single NVIDIA RTX 3090 GPU. To ensure fair comparisons, we followed the same experimental settings as U-KAN [13], including random seed initialization and evaluation protocol. For all datasets, the model was trained for 400 epochs with a batch size of 8 using the Adam optimizer, initialized at a learning rate of 1×10^{-4} and scheduled by cosine annealing to 1×10^{-5} . The loss function combines binary cross-entropy (BCE) and Dice loss to balance pixel-wise accuracy and region overlap. Standard data augmentations, including random rotation and flipping, were applied during training. Each dataset was randomly split into 80% training and 20% validation. To ensure robustness, Tab.1 and Tab.2 report results averaged over three independent runs with different random seeds (including data splits), while Tab.3–Tab.8 present single-run results obtained under a fixed seed to isolate the effect of each ablation. All FLOPs were measured on an input resolution of 512×512 to ensure consistent computational efficiency comparison across models. All experiments were conducted under this unified configuration.

4.3 Comparison with Common Segmentation Backbones

Tab. 1 compares GroupKAN with several established segmentation backbones on three benchmark datasets. We evaluate against convolution-based models (U-Net [6], U-Net++ [15]), attention-based approaches (Att-Unet [17], U-Mamba [22]), and MLP-style architectures (U-NeXt [20], Rolling-UNet [21]). U-KAN [13] is included as our primary baseline. GroupKAN achieves the highest performance in terms of both Intersection over Union (IoU) and F1 score across all datasets, demonstrating superior segmentation accuracy. As shown in Tab. 2, it also maintains a lightweight structure with fewer parameters and lower FLOPs than U-KAN (3.02M vs. 6.35M; 7.72 vs. 14.02 GFLOPs), while achieving a +1.11% improvement in IoU.

Qualitative results in Fig. 5 highlight GroupKAN’s ability to produce precise segmentation boundaries and preserve fine structural details. Compared to U-KAN and other baselines, GroupKAN more effectively handles both over- and under-segmentation, delivering improved delineation of complex anatomical regions. These visual results further reinforce GroupKAN’s effectiveness, demonstrating that GroupKAN serves as a strong backbone for medical image segmentation with a balanced trade-off between accuracy and efficiency.

To further validate the reliability of the observed performance gains, we conducted a one-sided Wilcoxon signed-rank test [35] over three independent runs across the BUSI, GlaS, and CVC datasets ($n = 9$ pairs). GroupKAN achieved significantly higher Intersection-over-Union (IoU) ($W = 39.0, p = 0.027$) and F1-score ($W = 45.0, p = 0.002$) than U-KAN, confirming that the improvements are statistically significant at the $p < 0.05$ level. This analysis further substantiates that GroupKAN’s performance gains are consistent and not due to random initialization or data split variations.

4.4 Ablation Studies

4.4.1 The Number of GKT Layer.

We assess the impact of GKT layer depth on segmentation performance. As shown in Tab. 3, the 3-layer configuration yields the highest IoU and F1, surpassing deeper variants. While increasing the number of GKT layers adds parameters

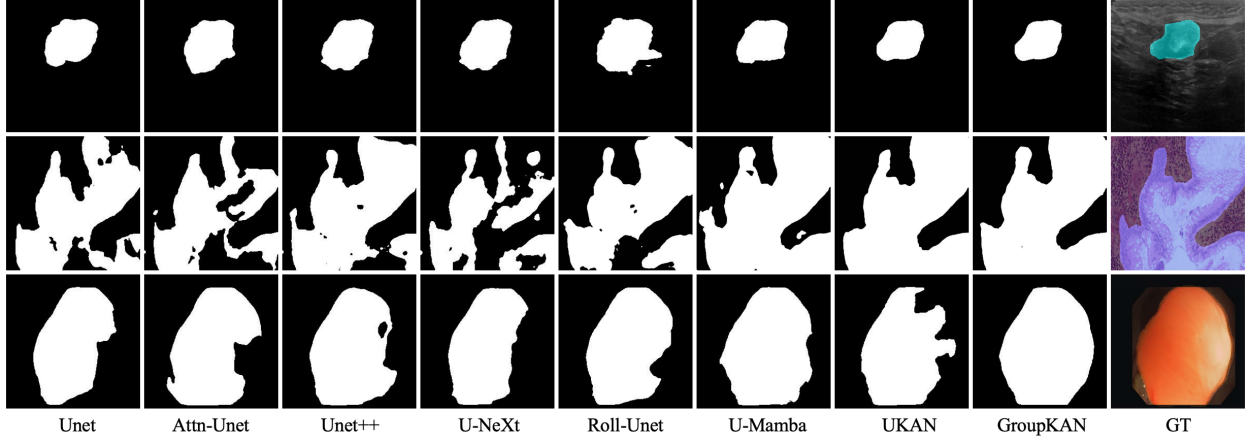


Figure 5: Qualitative comparison of segmentation results on BUSI, GlaS, and CVC-ClinicDB. GroupKAN produces more accurate and consistent masks across heterogeneous medical imaging modalities, closely aligning with the ground truth.

(up to 3.47M for 5 layers), it does not translate into better accuracy, likely due to overfitting or optimization instability. The 3-layer setup, with 3.02M parameters, achieves the best trade-off between accuracy and model complexity.

#GKT	IoU↑	F1↑	Params(M)
1 Layer	60.63	75.28	2.56
2 Layer	63.13	77.12	2.79
3 Layer	67.66	80.52	3.02
4 Layer	65.99	79.60	3.24
5 Layer	65.95	79.51	3.47

Table 3: Ablation study on the number of GKT layers in GroupKAN. The 3-layer variant achieves the highest IoU and F1 scores with moderate parameter overhead.

4.4.2 Impact of GKT vs. MLP.

We compare GKT- and MLP-based configurations, as shown in Table 4. The 3-layer GKT variant yields the highest IoU and F1 scores with moderate parameter count. Mixed configurations (e.g., MLP+GKT+GKT and GKT+MLP+GKT) exhibit slight drops in accuracy but still outperform the pure MLP baseline. Notably, the MLP $\times 3$ setup performs worst despite having more parameters. These results underscore the importance of GKT layers in enhancing segmentation accuracy while preserving model efficiency.

Model	IoU↑	F1↑	Params(M)
GKT $\times 3$	67.66	80.52	3.02
MLP+GKT+GKT	66.12	78.93	3.08
GKT+MLP+GKT	65.81	78.58	3.08
GKT+GKT+MLP	65.94	78.62	3.08
MLP $\times 3$	63.96	77.55	3.17

Table 4: Ablation study on the performance comparison between GKT and MLP models.

4.4.3 Hyperparameter Configurations.

We explore how IoU varies with parameter count under different hyperparameter settings, defined by G_{GKA} (groups in Grouped KAN Activation) and G_{GKT} (groups in Grouped KAN Transform), as shown in Fig. 6. The 3D plot visualizes each configuration using bubble size (parameters) and color (IoU), with dashed lines projecting points to the base plane at $Z = 62$. Among all combinations, the 16×16 setting, marked with a red star, achieves the highest IoU (67.66),

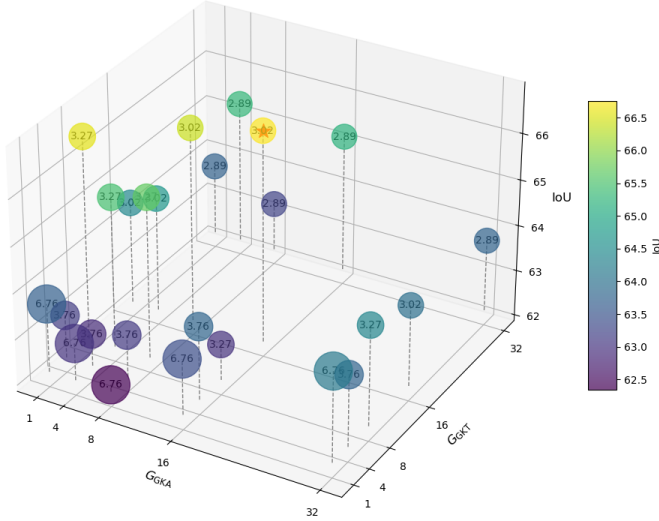


Figure 6: 3D visualization of IoU and parameter count across G_{GKA} and G_{GKT} configurations. Bubble size indicates model size (M), color represents IoU, and the red star marks the optimal setting.

balancing segmentation accuracy and model complexity. Notably, overly coarse or overly fine groupings degrade performance, indicating the necessity of tuning group granularity. These results highlight the sensitivity of grouped configurations and their central role in optimizing model design.

4.4.4 Model Scaling.

We investigate model scaling by varying the channel dimensions C_1 , C_2 , and C_3 in GroupKAN (see Table 5). Larger models consistently yield higher IoU and F1, at the cost of increased parameters and computation. The default GroupKAN configuration achieves a strong balance between performance and efficiency, while GroupKAN-S provides a lightweight alternative with only minor accuracy trade-offs.

Model	C_1	C_2	C_3	IoU^\uparrow	F1^\uparrow	Params
G-KAN-S	64	96	128	65.89	79.29	0.87
G-KAN	128	160	256	67.66	80.52	3.02
G-KAN-L	256	320	512	68.36	80.95	12.00

Table 5: Ablation on model scaling via encoder channels (C_1 , C_2 , C_3) in GroupKAN. “G-KAN” refers to the base GroupKAN model; G-KAN-S and G-KAN-L are its small and large variants.

4.4.5 Effect of GKA.

Compared to both fixed (ReLU [25], GELU [26]) and learnable (TeLU [27], GoLU [28]) activations, our GKA consistently yields superior results, particularly in F1-score, which reflects better delineation of fine structures. We further observe that inserting activations after patch embedding improves all variants, with the greatest gains seen in our method. These findings highlight the benefit of structured, group-aware activations in dense medical image segmentation.

Effect of GKT

We ablate the Grouped KAN Transform (GKT) and its convolutional components to analyze their effects. Removing the 1×1 pointwise convolution reduces performance (IoU 0.6552, Dice 0.7890) and decreases parameters to 2.61M. Removing the 3×3 depthwise convolution further degrades accuracy (IoU 0.6246, Dice 0.7666, 2.99M). Excluding GKT entirely gives the lowest scores (IoU 0.6015, Dice 0.7483, 2.77M). The complete configuration with both convolutions

Activation Function	IoU↑	F1↑
None	66.10	78.22
ReLU [25]	66.63	79.24
GELU [26]	66.45	79.46
GoLU [28]	66.84	79.82
TeLU [36]	66.44	79.22
GKA (Ours)	67.66	80.52

Table 6: Comparison of activation functions after patch embedding. GKA (ours) outperforms fixed (ReLU, GELU) and learnable (TeLU, DyT) variants in IoU and F1.

Configuration	IoU	Dice	Params (M)
No 1×1 PWConv	0.6552	0.7890	2.61
No 3×3 DWConv	0.6246	0.7666	2.99
No GKT	0.6015	0.7483	2.77
GKT (with PW+DW)	0.6766	0.8052	3.02

Table 7: Ablation on the effect of GKT and associated convolutions. GKT provides the main functional transformation, while PWConv and DWConv enhance inter-group and spatial interactions.

achieves the best performance (IoU 0.6766, Dice 0.8052, 3.02M). These results confirm that GKT is essential for accurate feature transformation, while PWConv and DWConv support cross-group and spatial interactions, respectively. These results demonstrate that GKT improves segmentation accuracy with minimal parameter overhead, reflecting its parameter efficiency.

4.4.6 Explainability Analysis.

We further evaluate the interpretability of GroupKAN by analyzing activation patterns (Fig. 7). The *top-left* image (U-KAN) fails to localize the region of interest, with a plausibility IoU of 0.41. The *top-right* variant (GroupKAN w/o GKT) performs worse (0.28), indicating degraded focus without GKT. Incorporating GKT (*bottom-left*) improves alignment with the ground truth, achieving a plausibility IoU of 0.52. The *bottom-right* shows the GT mask.

To further validate these findings, we report average Plausibility IoU across the test set (Tab. 8). U-KAN achieves 0.465, GroupKAN without GKT drops to 0.281, while GroupKAN with GKT reaches 0.517. These results confirm that GKT enhances activation-ground truth consistency and improves interpretability in segmentation.

Method	Average Plausibility IoU
U-KAN	0.465
Ours w/o GKT	0.281
Ours w/ GKT	0.517

Table 8: Average Plausibility IoU comparison on the test set. GKT improves activation alignment and interpretability.

5 Conclusion

In this work, we propose GroupKAN, a lightweight segmentation network leveraging group-structured spline modeling for medical image segmentation. It incorporates *Grouped KAN Activation* to model token-wise nonlinearity and *Grouped KAN Transform* for efficient group-wise channel interaction, reducing the complexity of the KAN layer in U-KAN from $\mathcal{O}(C^2)$ to $\mathcal{O}(C^2/G)$. On BUSI, GlaS, and CVC benchmarks, GroupKAN serves as a strong backbone, achieving 79.80% average IoU while using only 47.6% of U-KAN’s parameters (3.02 M vs. 6.35 M). In addition, plausibility IoU evaluations show improved alignment between activation maps and ground truth, supporting the interpretability of GroupKAN in clinical segmentation. This establishes a new paradigm for lightweight and interpretable clinical segmentation.

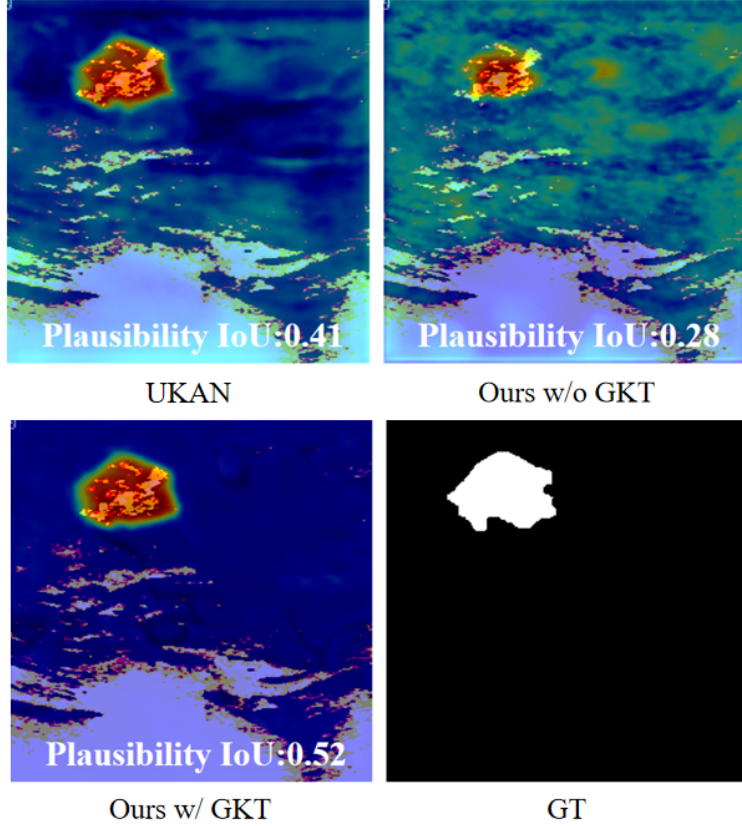


Figure 7: Channel activation maps for explainability comparison. GroupKAN with GKT (bottom-left) shows the best alignment with the GT mask (bottom-right), achieving the highest plausibility IoU (0.52). U-KAN and GroupKAN w/o GKT yield lower alignment, highlighting GKT’s role in improving interpretability.

References

- [1] Risheng Wang, Tao Lei, Ruixia Cui, Bingtao Zhang, Hongying Meng, and Asoke K Nandi. Medical image segmentation using deep learning: A survey. *IET image processing*, 16(5):1243–1267, 2022.
- [2] KKD Ramesh, G Kiran Kumar, K Swapna, Debabrata Datta, and S Suman Rajest. A review of medical image segmentation algorithms. *EAI Endorsed Transactions on Pervasive Health & Technology*, 7(27), 2021.
- [3] Sohaib Asif, Yi Wenhui, Saif ur Rehman, Qurrat ul ain, Kamran Amjad, Yi Yueyang, Si Jinhai, and Muhammad Awais. Advancements and prospects of machine learning in medical diagnostics: unveiling the future of diagnostic precision. *Archives of Computational Methods in Engineering*, 32(2):853–883, 2025.
- [4] Yuhang Zhang, Xiao Ma, Mingchao Li, Kun Huang, Jie Zhu, Miao Wang, Xi Wang, Menglin Wu, and Pheng-Ann Heng. Generalist medical foundation model improves prostate cancer segmentation from multimodal mri images. *npj Digital Medicine*, 8(1):372, 2025.
- [5] Enerst Edozie, Aliyu Nuhu Shuaibu, Ukaigwu Kelechi John, and Bashir Olaniyi Sadiq. Comprehensive review of recent developments in visual object detection based on deep learning. *Artificial Intelligence Review*, 58(9):277, 2025.
- [6] Olaf Ronneberger, Philipp Fischer, and Thomas Brox. U-net: Convolutional networks for biomedical image segmentation. In *International Conference on Medical image computing and computer-assisted intervention*, pages 234–241. Springer, 2015.
- [7] Md Maruf Hossain Shuvo, Syed Kamrul Islam, Jianlin Cheng, and Bashir I Morshed. Efficient acceleration of deep learning inference on resource-constrained edge devices: A review. *Proceedings of the IEEE*, 111(1):42–91, 2022.

- [8] Abolfazl Younesi, Mohsen Ansari, Mohammadamin Fazli, Alireza Ejlali, Muhammad Shafique, and Jörg Henkel. A comprehensive survey of convolutions in deep learning: Applications, challenges, and future trends. *IEEE Access*, 12:41180–41218, 2024.
- [9] Weizhe Hua, Zihang Dai, Hanxiao Liu, and Quoc Le. Transformer quality in linear time. In *International conference on machine learning*, pages 9099–9117. PMLR, 2022.
- [10] Quentin Fournier, Gaétan Marceau Caron, and Daniel Aloise. A practical survey on faster and lighter transformers. *ACM Computing Surveys*, 55(14s):1–40, 2023.
- [11] Yehjin Shin, Jeongwhan Choi, Hyowon Wi, and Noseong Park. An attentive inductive bias for sequential recommendation beyond the self-attention. In *Proceedings of the AAAI conference on artificial intelligence*, volume 38, pages 8984–8992, 2024.
- [12] Albert Gu and Tri Dao. Mamba: Linear-time sequence modeling with selective state spaces. *arXiv preprint arXiv:2312.00752*, 2023.
- [13] Chenxin Li, Xinyu Liu, Wuyang Li, Cheng Wang, Hengyu Liu, Yifan Liu, Zhen Chen, and Yixuan Yuan. U-kan makes strong backbone for medical image segmentation and generation. In *Proceedings of the AAAI Conference on Artificial Intelligence*, volume 39, pages 4652–4660, 2025.
- [14] Ziming Liu, Yixuan Wang, Sachin Vaidya, Fabian Ruehle, James Halverson, Marin Soljačić, Thomas Y Hou, and Max Tegmark. Kan: Kolmogorov-arnold networks. *arXiv preprint arXiv:2404.19756*, 2024.
- [15] Zongwei Zhou, Md Mahfuzur Rahman Siddiquee, Nima Tajbakhsh, and Jianming Liang. Unet++: A nested u-net architecture for medical image segmentation. In *International workshop on deep learning in medical image analysis*, pages 3–11. Springer, 2018.
- [16] Zichen Luo, Xinshan Zhu, Lan Zhang, and Biao Sun. Rethinking u-net: Task-adaptive mixture of skip connections for enhanced medical image segmentation. In *Proceedings of the AAAI Conference on Artificial Intelligence*, volume 39, pages 5874–5882, 2025.
- [17] Ozan Oktay, Jo Schlemper, Loic Le Folgoc, Matthew Lee, Mattias Heinrich, Kazunari Misawa, Kensaku Mori, Steven McDonagh, Nils Y Hammerla, Bernhard Kainz, et al. Attention u-net: Learning where to look for the pancreas. *arXiv preprint arXiv:1804.03999*, 2018.
- [18] Yanfeng Zhou, Lingrui Li, Le Lu, and Minfeng Xu. nnwnet: Rethinking the use of transformers in biomedical image segmentation and calling for a unified evaluation benchmark. In *Proceedings of the Computer Vision and Pattern Recognition Conference*, pages 20852–20862, 2025.
- [19] Fuchen Zheng, Xuhang Chen, Weihuang Liu, Haolun Li, Yingtie Lei, Jiahui He, Chi-Man Pun, and Shoujun Zhou. Smaformer: Synergistic multi-attention transformer for medical image segmentation. In *2024 IEEE International Conference on Bioinformatics and Biomedicine (BIBM)*, pages 4048–4053. IEEE, 2024.
- [20] Jeya Maria Jose Valanarasu and Vishal M Patel. Unext: Mlp-based rapid medical image segmentation network. In *International conference on medical image computing and computer-assisted intervention*, pages 23–33. Springer, 2022.
- [21] Yutong Liu, Haijiang Zhu, Mengting Liu, Huaiyuan Yu, Zihan Chen, and Jie Gao. Rolling-unet: Revitalizing mlp’s ability to efficiently extract long-distance dependencies for medical image segmentation. In *Proceedings of the AAAI conference on artificial intelligence*, volume 38, pages 3819–3827, 2024.
- [22] Jun Ma, Feifei Li, and Bo Wang. U-mamba: Enhancing long-range dependency for biomedical image segmentation. *arXiv preprint arXiv:2401.04722*, 2024.
- [23] Alexander Dylan Bodner, Antonio Santiago Tepsich, Jack Natan Spolski, and Santiago Pourteau. Convolutional kolmogorov-arnold networks. *arXiv preprint arXiv:2406.13155*, 2024.
- [24] Ivan Drokin. Kolmogorov-arnold convolutions: Design principles and empirical studies. *arXiv preprint arXiv:2407.01092*, 2024.
- [25] Vinod Nair and Geoffrey E Hinton. Rectified linear units improve restricted boltzmann machines. In *Proceedings of the 27th international conference on machine learning (ICML-10)*, pages 807–814, 2010.
- [26] Dan Hendrycks and Kevin Gimpel. Gaussian error linear units (gelus). *arXiv preprint arXiv:1606.08415*, 2016.
- [27] Alfredo Fernandez. Telu activation function for fast and stable deep learning. Master’s thesis, University of South Florida, 2024.
- [28] Anirban Das, Siddharth Rao, and Tirthankar Bhattacharya. Gompertz linear units: Leveraging asymmetry for enhanced learning dynamics. *arXiv preprint arXiv:2502.03654*, 2025.

- [29] Haiping Wu, Bin Xiao, Noel Codella, Mengchen Liu, Xiyang Dai, Lu Yuan, and Lei Zhang. CvT: Introducing convolutions to vision transformers. In *Proceedings of the IEEE/CVF international conference on computer vision*, pages 22–31, 2021.
- [30] Wenhui Wang, Enze Xie, Xiang Li, Deng-Ping Fan, Kaitao Song, Ding Liang, Tong Lu, Ping Luo, and Ling Shao. Pvt v2: Improved baselines with pyramid vision transformer. *Computational visual media*, 8(3):415–424, 2022.
- [31] Andrei Nikolaevich Kolmogorov. On the representations of continuous functions of many variables by superposition of continuous functions of one variable and addition. In *Dokl. Akad. Nauk USSR*, volume 114, pages 953–956, 1957.
- [32] Walid Al-Dhabyani, Mohammed Gomaa, Hussien Khaled, and Aly Fahmy. Dataset of breast ultrasound images. *Data in brief*, 28:104863, 2020.
- [33] Korsuk Sirinukunwattana, Josien PW Pluim, Hao Chen, Xiaojuan Qi, Pheng-Ann Heng, Yun Bo Guo, Li Yang Wang, Bogdan J Matuszewski, Elia Bruni, Urko Sanchez, et al. Gland segmentation in colon histology images: The glas challenge contest. *Medical image analysis*, 35:489–502, 2017.
- [34] Jorge Bernal, F Javier Sánchez, Gloria Fernández-Esparrach, Debora Gil, Cristina Rodríguez, and Fernando Vilariño. Wm-dova maps for accurate polyp highlighting in colonoscopy: Validation vs. saliency maps from physicians. *Computerized medical imaging and graphics*, 43:99–111, 2015.
- [35] Frank Wilcoxon. Individual comparisons by ranking methods. *biometrics bulletin*, 1 (6), 80-83, 1945.
- [36] Jiachen Zhu, Xinlei Chen, Kaiming He, Yann LeCun, and Zhuang Liu. Transformers without normalization. In *Proceedings of the Computer Vision and Pattern Recognition Conference*, pages 14901–14911, 2025.